Scanning Tunneling Microscopy Reveals Single-Molecule Insights into the Self-Assembly of Amyloid Fibrils

Nataliya Kalashnyk,[†,∥,¶] Jakob T. Nielsen,[‡,¶] Erik H. Nielsen,[‡] Troels Skrydstrup,[‡] Daniel E. Otzen,[§] Erik Lægsgaard,[†] Chen Wang,[⊥] Flemming Besenbacher,[†] Niels Chr. Nielsen,[‡,*] and Trolle R. Linderoth[†,*]

[†]Sino-Danish Center for Molecular Nanostructures on Surfaces, Interdisciplinary Nanoscience Center (iNANO) and Department of Physics and Astronomy, Aarhus University, DK-8000 Aarhus C, Denmark, [‡]Center for Insoluble Protein Structures (inSPIN), Interdisciplinary Nanoscience Center (iNANO) and Department of Chemistry, Aarhus University, DK-8000 Aarhus C, Denmark, [§]Center for Insoluble Protein Structures (inSPIN), Interdisciplinary Nanoscience Center (iNANO) and Department of Molecular Biology and Genetics, Aarhus University, DK-8000 Aarhus C, Denmark, and [⊥]Sino-Danish Center for Molecular Nanostructures on Surfaces, National Center for Nanoscience and Technology (NCNST), No 11, Beiyitiao Zhongguancun, Beijing, People's Republic of China. [¶]These authors contributed equally to this work. [∥]Present address: Department of Chemistry, University of Warwick, Gibbet Hill Road, Coventry, CV4 7AL, United Kingdom.

ABSTRACT

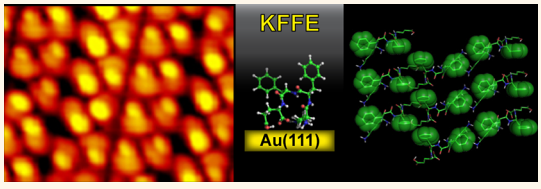

Many severe diseases are associated with amyloid fibril deposits in the body caused by protein misfolding. Structural information on amyloid fibrils is accumulating rapidly, but little is known about the assembly of peptides into fibrils at the level of individual molecules. Here we investigate self-assembly of the fibril-forming tetrapeptides KFFE and KVVE on a gold surface under ultraclean vacuum conditions using scanning tunneling microscopy. Combined with restrained molecular dynamics modeling, we identify peptide arrangements with interesting similarities to fibril structures. By resolving individual peptide residues and revealing conformational heterogeneities and dynamics, we demonstrate how conformational correlations may be involved in cooperative fibril growth. Most interestingly, intermolecular interactions prevail over intramolecular interactions, and assembly of the phenyl-rich KFFE peptide appears not to be dominated by $\pi-\pi$ interactions. This study offers interesting perspectives for obtaining fundamental single-molecule insights into fibril formation using a surface science approach to study idealized model systems.

KEYWORDS: scanning tunneling microscopy · Au(111) · biomolecular adsorption · peptides · molecular self-assembly · restrained molecular dynamics modeling ·

Amyloid fibrils resulting from protein misfolding are involved in multiple neurodegenerative disorders, such as Alzheimer's and Parkinson's disease.[1] Microscopically, fibrils consist of peptide strands connected by hydrogen bonding into β-sheets, which associate laterally through hydrophobic interactions between the side chains. Numerous studies have been performed to gain insight into the detailed organization and formation of fibrillar structures, predominantly using techniques such as X-ray diffraction,[2] cryo-EM,[3,4] and solid-state NMR spectroscopy.[5−8] These averaging techniques yield good statistical structural models with resolution down to the angstrom level but provide only limited structural insight into local heterogeneities and the role of individual molecules in the assembly process. In contrast, scanning probe microscopies reveal the real-space, atomic-scale realm of matter by imaging individual molecules adsorbed on surfaces. Using such methods, complementary information may therefore be gained on amyloid fibrillation. Larger fibril aggregates have been investigated with atomic force microscopy,[9,10] and in recent studies, scanning tunneling microscopy (STM) was employed to image aggregation of oligopeptide lamellae at the liquid−solid interface,[11−17] however, without discriminating individual residues on the peptide chains. At a yet more fundamental level, the self-assembly of biomolecular building blocks, such as DNA bases or simple amino acids,[18−22] has been studied on metal surfaces under ultrahigh vacuum (UHV) conditions, providing fundamental insights into principles for biomolecular interaction and organization. Such STM studies relying on thermal sublimation to deposit molecules on the surface have for peptides so far been extended to dialanine and diphenylalanine.[23−26]

Here we demonstrate how UHV-STM can be used to obtain single-molecule insights into assembly processes relevant for amyloid fibrillation. We have studied the two tetrapeptides KFFE and KVVE (Figure 1),

* Address correspondence to trolle@inano.au.dk, ncn@inano.au.dk.

Received for review April 18, 2012 and accepted July 2, 2012.

Published online July 10, 2012
10.1021/nn301708d

previously identified to be among the minimal peptide units forming amyloid fibrils *in vitro*.[27,28] These peptides are terminated by the same lysine (K) and glutamate (E) residues (both having high β-sheet pair correlation) but differ in the two central residues, which are phenylalanine (F) and valine (V), respectively. This structural difference allows us to address the importance of $\pi-\pi$ interactions for the assembly process. We find that these tetrapeptides form highly ordered adsorption structures on the inert Au(111) surface under the ultraclean, solvent-free UHV conditions. The high-resolution STM results, in particular, reveal two distinct patterns with parallel/antiparallel arrangement of the tetrapeptide chains, showing interesting similarities to fibrillar structures. These STM structures are modeled using a method applying restrained molecular dynamics and an empirical force field (henceforth termed the restrained MDFF method).[29] Very interestingly, the high-resolution STM images allow individual residues on the peptide chains to be identified and reveal heterogeneities at the single-molecule level and dynamic changes between residue conformations. From a thorough statistical analysis of two distinct conformational states for the F/V side chains, clear intermolecular correlations between the different conformations are revealed, leading us to propose a mechanism for cooperative fibrillar growth.

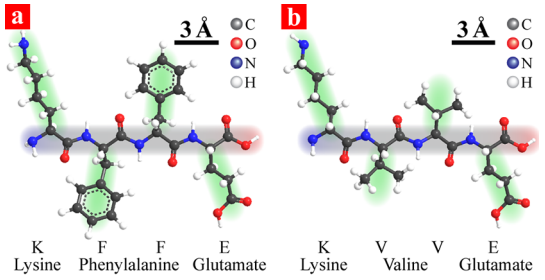

Figure 1. Ball and stick models of the tetrapeptides KFFE (a) and KVVE (b). Both tetrapeptides consist of a peptide backbone (indicated by gray shadow) with an N-terminus (blue shadow) and a C-terminus (red shadow). Four side groups (green shadows) extend from the peptide backbone. The peptide chains of KFFE and KVVE bear the same side groups at the ends originating from lysine (Lys, K) and glutamate (Glu,E) while they differ in the two side groups at their centers which originate from phenylalanine (Phe, F) and valine (Val, V), respectively.

RESULTS AND DISCUSSION

KFFE Row Structure: STM Observations. Figure 2a shows an STM image of the interior of a molecular island observed on the Au(111) surface after deposition of KFFE. The island has a regular structure consisting of parallel rows oriented along the [11$\bar{2}$] substrate direction and formed from characteristic double protrusions. To identify individual peptide units within this structure, we examined point defects and island perimeters as depicted in the STM image in Figure 2b. The molecular rows are terminated by dumbbell-shaped features, which are clearly isolated from the surrounding disordered structure in the uppermost part of the image and which have a length of ~12 Å, corresponding well to the length of the extended peptide backbone of KFFE. We therefore assign each dumbbell-shaped feature to an individual peptide molecule. The high-resolution STM images show that the peptide units are composed of two double protrusions, each consisting of a larger protrusion overlaid by a smaller brighter part (indicated by black circles and smaller black ovals, respectively, in Figure 2a). We tentatively

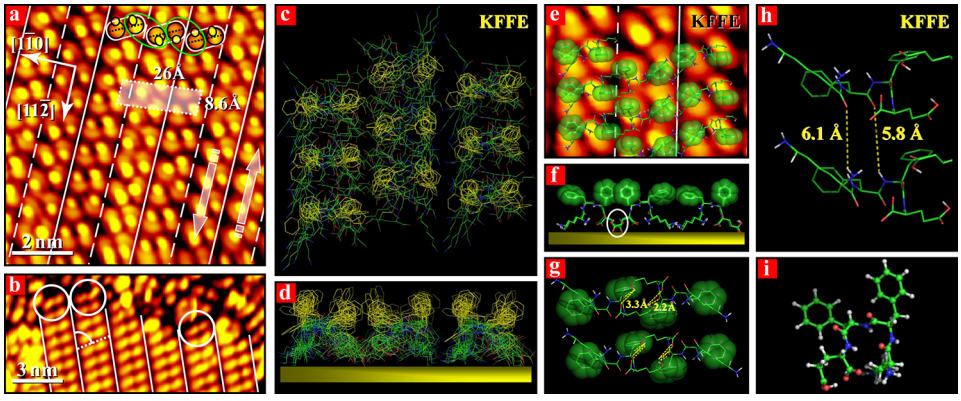

Figure 2. Row structure for KFFE on the Au(111) surface. (a) STM image with oblique unit cell (26 Å × 8.6 Å) and lattice directions indicated. Individual peptides are marked by white oval contours. Solid/dashed lines indicate the two types of row boundaries, differing by the relative orientation (see green ovals) of the bright protrusions attributed to Phe residues. (b) STM image of domain boundary (row terminations are marked by circles). (c–i) MDFF structural models. (c) Top view of a superposition of the 10 lowest energy structures with Phe side chains highlighted in yellow. (d) Same in side view with the Au surface indicated by yellow bar. (e) Best representative model superimposed on an STM image with Phe side chains highlighted in green. (f) Same in side view; white oval indicates putative surface binding. (g) Same in top view; yellow dashed lines indicate possible hydrogen bonds between main chain and Glu side chain acid groups in adjacent rows. (h) Close-up of two neighboring monomers along a row, indicating shortest distance between main chain hydrogen bond donors and acceptors with yellow dashes. (i) KFFE monomer shown in ball and stick representation. Carbon (green), nitrogen (blue), oxygen (red), hydrogen (white).

assign the bright protrusions to the two electron-rich phenylalanine (F) moieties and the less bright protrusions to the peptide backbones. No protrusions which can be attributed to the lysine (K) and glutamate (E) residues are observed. The bright protrusions are located off-center compared to the larger less bright protrusions, the positions of the bright protrusions are correlated such that both protrusions on a given molecule are located at the same side of the molecular axis; all molecules in a given row have their protrusions located to the same side. The rows thus alternatingly have protrusions pointing upward or downward along the row axis, as indicated by arrows in Figure 2a. Neighboring molecules in adjacent rows are thus related by a C_2 rotation, creating two types of inter-row boundaries where the bright protrusions point either toward each other (solid white lines) or in opposite directions (dashed white lines).

KFFE Row Structure: Restrained MDFF Modeling. To gain further insight from these high-resolution STM images, we modeled the observed tetrapeptide structures. This is challenging due to the large surface unit cell and the complexity of the many possible molecular arrangements and conformations. Motivated by modeling of protein structures, which is commonly performed by the restrained MDFF method using structural constraints derived from NMR data,[29,30] we used a similar approach to model the STM observations. The MDFF method relies on simulated annealing which is a global optimization technique particularly well suited for large search spaces.[31,32] In the present context, the peptide geometry search space was traveled following Newton's laws of motion to optimize an energy function which incorporates an empirical force field together with constraints for distances and symmetries. The empirical force field rewards favorable bond lengths, angles, and dihedral angles and prevents clashes between atoms by harmonic potentials. The constraints included translational symmetry along the rows and rotational symmetry between the rows (imposed as described previously for a fibril structure[7]). In addition, distances between identical groups related by translational and rotational symmetry were derived from STM images and applied as distance restraints. The present case is, to our knowledge, the first where the MDFF method has been used with constraints derived from STM data. The surface atoms were not included in the simulations, but two-dimensional confinement was modeled indirectly using a planarity restraint requiring all atoms be within ± 5 Å from a fixed plane. For the row structure, the N/O atoms from the Lys/Glu side chains and the N/C peptide chain terminals were furthermore required to be within ± 1 Å from a common plane, which was allowed to move during the annealing. This reflects the assumption that the polar atoms of the side chains and the end groups point toward the surface. In the modeling of the structures, we also took into account the observation of conformational freedom for the Phe residues, as discussed further below. We analyzed a large ensemble of models (800 for each structure), and the models with the lowest combined force field and restraint energy in combination with best visual fit to the STM images were selected for further analysis.

Figure 2c–h summarizes the results from the MDFF calculations of the KFFE row structure. Overlays of the 10 lowest energy structures are shown in Figure 2c (top view) and Figure 2d (side view along direction of the rows). The Phe groups point away from the surface, and the molecules generally adopt a U-shaped conformation where the backbone is bent and the Glu and Lys residues as well as their N-amino and C-carboxyl groups point toward the surface. All 10 models are consistent with respect to the position of the Phe groups, and the Phe group positions correlate very well with the protrusions in the STM images. In Figure 2e, the model which correlates best with the STM results is shown superimposed on an STM image (side view in Figure 2f). The bent conformation (Figure 2i) makes the KFFE molecule sufficiently compact to fit the experimentally observed periodicity across the rows and may explain why the Lys and Glu side chains are not revealed in the STM images. This model is also in good correspondence with previous theoretical studies[33–35] showing a U-shaped conformation to be preferred for isolated KFFE peptides. The two distinct row interfaces involve Lys–Lys and Glu–Glu interaction. It is observed in the models that Phe rings are in contact across the row interfaces sterically restricting the conformational freedom of the Phe side chain. Possibly, hydrogen bonds between the protonated Glu side chain and main chain C-terminal carboxylic acid groups of opposite rows (white circle in Figure 2f and yellow lines in Figure 2g) stabilize the row interface. Conversely, the peptides are less densely packed along the rows with the Phe side chains further apart compared to the inter-row interactions. Peptide neighbors along the rows are in favorable orientation to form hydrogen bonds, but the distance between amide proton and carbonyl oxygen of ~6 Å (see Figure 2h) is considerably larger than the 2–3 Å expected for canonical hydrogen bonds in solvated states as observed in, for example, amyloid fibrils. The observed geometry might nevertheless represent a structural precursor to the formation of fibrils, possibly arrested at larger peptide chain separation by interaction with the substrate.

KVVE Antiparallel Structure: STM Observations. While the row structure is the only structure observed for KFFE upon deposition at room temperature, three additional structures were observed for the KVVE peptide. Here we focus on one of these, shown in Figure 3a (see Figure S3 in Supporting Information for STM images of the other two structures). This *antiparallel structure*

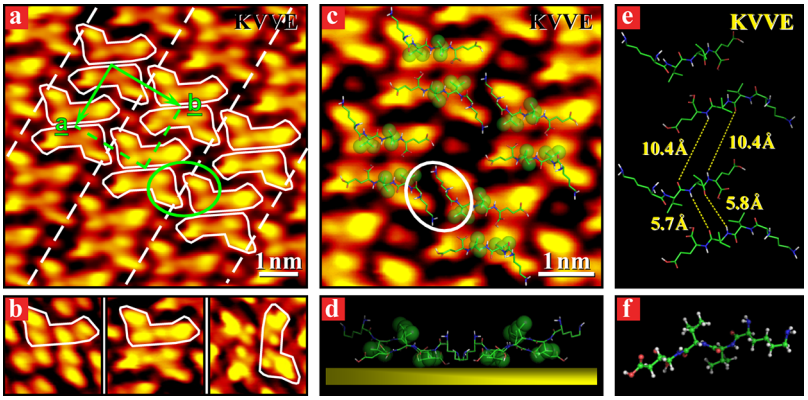

Figure 3. Antiparallel structure of KVVE on the Au(111) surface. (a) STM image with individual peptide units indicated by white L-shaped outlines. Rectangular unit cell of 18.3 Å × 21.4 Å dimension is shown in green. (b) STM images of the antiparallel row motif registered under three STM imaging conditions showing individual residues (see text). (c−e) Best representative MDFF structural model shown with Val side chain carbons highlighted by green transparent spheres (see Figure S2 for overlay of 10 lowest energy structures). (c) Top view overlaid on the STM image. White oval indicates antiparallel organization of the Lys side chain. (d) Side view with Au surface indicated by yellow bar. (e) Close-up of neighboring tetrapeptides, highlighting shortest distance between main chain hydrogen bond donors and acceptors with yellow dashes. (f) Single monomer shown with ball and stick representation. Color coding as in Figure 2.

consists of rotor-shaped features each formed from two L-shaped units (indicated by white outlines) mutually rotated by 180° and stacked back-to-back in antiparallel arrangement with their long legs close-packed. The rotor-shaped features stack into rows as indicated by white dashed lines. Between the rows, the short legs of the L-shaped units come in close proximity of each other. The structure has been observed in three different STM imaging modes, as depicted in Figure 3b. (The imaging modes are attributed to different STM tip states, possibly caused by attachment of molecules or fragments at the tip apex.) In the most frequent imaging mode (leftmost panel in Figure 3b), we observe four distinct protrusions for each L-shaped peptide, and we assign these protrusions to individual residues of the tetrapeptide. For the second imaging mode (middlemost panel of Figure 3b and the STM image of Figure 3a), a single tetrapeptide molecule is imaged as two bright, elongated outer protrusions interconnected by a less bright central part. The elongated bright protrusion at the short leg of the L-shaped unit has a length of ~6.9 Å, which corresponds well to the dimension of a fully stretched lysine chain. The protrusion terminating the long leg of the L-shaped unit is smaller and attributed to Glu. In the third imaging mode (right panel of Figure 3b), two distinct bright protrusions are revealed on the central portion of the molecular structure which we attribute to the Val side chains, similarly to the case for the row structure. Importantly, the unprecedented identification of all four residues on the tetrapeptide chain from the high-resolution STM images demonstrates that it is indeed possible to thermally deposit these relatively large peptide units on the 2D gold surface without loss of residues due to fragmentation.

KVVE Antiparallel Structure: MDFF Modeling. To extract further structural insight from the STM results for the KVVE antiparallel row structure, we modeled it by the MDFF method. In contrast to the case for the row structure, no additional restrictions were employed for the polar groups. A superposition of the 10 lowest energy structures provides a convincing visual similarity to the rotor-shaped features observed in the STM images (see Figure S2g). Figure 3c shows one of these structures overlaid on an STM image. The model agrees very well with the assignment of STM features to individual residues as discussed above. A side view of this model (Figure 3d) shows that, in comparison to the case for the KFFE row structure (Figure 2f), the molecules are adsorbed in a more outstretched adsorption conformation, probably allowing the high degree of detail in resolving individual residues on the tetrapeptide chain. The peptide chain assumes an S-shape with the side chains alternatingly pointing toward and away from the surface, and the carboxyl groups are oriented toward the substrate (Figure 3d). The most interesting aspect of the MDFF structural model is the S-shaped (β-strand-like) molecular conformation (Figure 3d) and the antiparallel arrangement of neighboring peptide backbones, which are features qualitatively resembling earlier proposed fibril structures.[36,37] However, the distances between the antiparallel KVVE backbones within (5.8 Å) and between (10.4 Å) the rotor-shaped units are too large to allow significant hydrogen bonding as was also found for the row structures (see Figure 3e).

Phe/Val Residue Conformations in the KFFE/KVVE Row Structures. A major aspect of the local probe STM investigation of fibril-like molecular assemblies is the ability to address local structural heterogeneities and propagation of structural order. Close inspection of STM images for the KFFE row structure (Figure 2a) reveals that the protrusions attributed to the Phe moieties appear with different brightness. From a detailed quantitative

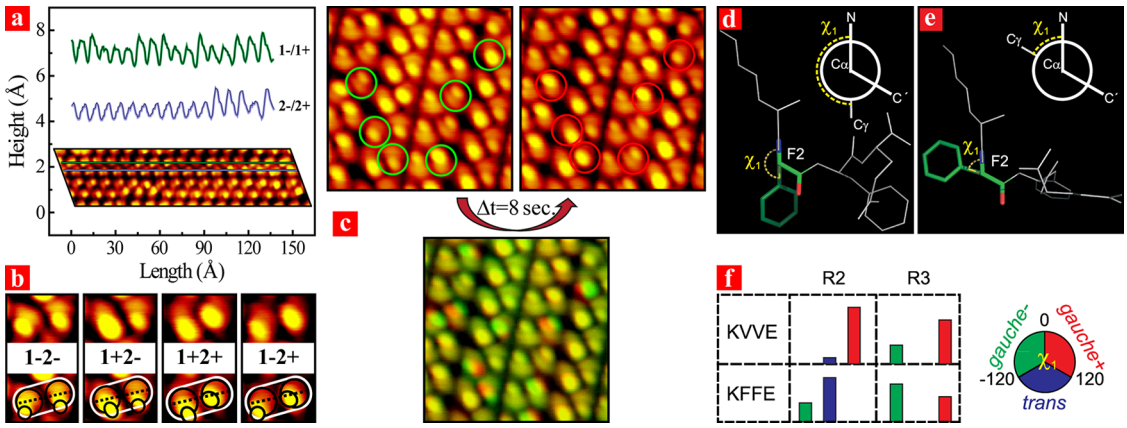

Figure 4. Analysis of conformations for Phe/Val side chains in KFFE/KVVE row structures. (a) STM height profiles of KFFE row structure acquired along the row direction as indicated, showing distinct high/low states for the bright protrusions attributed to Phe residues (STM image rotated to make the peptide rows horizontal). (b) STM close-ups and schematic models of the four possible combinations of high/low states on a KFFE unit. Double protrusions are referred to as 1 and 2 depending on their position when the peptide units are oriented horizontally with the bright off-axis protrusions pointing downward (note that peptide orientation changes between adjacent rows). (c) STM images of the same region of the KFFE row structure acquired with a time separation of 8 s and at a surface temperature of 140 K. Groups that change conformation are indicated by green/red circles. At the bottom is shown a color addition overlay of the two images in green and red color scale, respectively, such that stationary protrusions appear approximately yellow and initial/final positions appear in green/red. (d,e) Details of MDFF models for the KFFE row structure. A single monomer is shown looking down the Phe_2 Cα−Cβ bond with N of Phe_2 pointing toward the top of the page (Phe_2 unit highlighted with sticks; color coding as in Figure 2). The χ_1 dihedral angle for Phe_2 is indicated with yellow dashes, showing *gauche*− (d) and *trans* (e) conformations, respectively (χ_1 defined by Newman projections). (f) Statistics for the χ_1 dihedral angle obtained from analysis of the 10 lowest energy structures of the parallel row structures of KVVE/KFFE. Histograms show the fraction of observations of the three different possible values for χ_1 for R_2 (left column) and R_3 (right column), where R indicates Phe or Val as appropriate (right: definition/color-coding of the conformational categories based on the dihedral angle).

analysis of STM height profiles through the peptide rows (see Figure 4a), we conclude that the protrusions can be assigned to two distinct classes, which we denote as either "high" (+) or "low" (−) with a difference in apparent height of 0.8 ± 0.3 Å (note that the apparent height in STM scans is not a measure of true physical height but also carries contributions from electronic density of states and tunneling conductivity). The observation of two distinct states for each Phe residue leads to four combinatorial possibilities for each peptide unit, all of which are observed as illustrated in Figure 4b. The high/low protrusions differ slightly in their position with respect to the larger underlying subprotrusions as indicated by the positions of the smaller ovals compared to the larger circles in the schematic of Figure 4b. Analysis of the similar KVVE row structure also shows that the protrusions attributed to the Val residues can be observed in two distinct states.

The dynamic evolution of the KFFE row structure was followed by acquiring consecutive time-lapsed STM images of the same region of the surface. As illustrated in Figure 4c, the individual bright protrusions can change between the high/low states, and we thus attribute the two brightness levels to different conformational states of the Phe moieties and the observed changes to thermally induced conformational dynamics. This hypothesis is supported by our structural models: Following the conventional grouping of the torsion angle χ_1 (see Figure 4d,e) for the Phe/Val side chains into three rotameric forms (see definition of intervals in Figure 4f),[38] analysis of the 10 lowest energy structures reveals that χ_1 preferentially adopts two of these (see Figure 4f). It was not possible to directly assign the high/low states observed in the STM images to the proposed molecular conformations, but the analysis suggests that the high state does not necessarily result from the same residue conformation for the two Phe residues of a KFFE unit. Similarly, the molecular basis for the high/low states may be different for the Phe and Val residues.

Correlation Analysis for Residue Conformations. To obtain quantitative information on the occurrence of the high/low conformational states and possible intra- and intermolecular correlations between them, we carefully analyzed STM images for the KFFE and KVVE row structures. Results for a total of ~888 peptide units are summarized in Table 1 and Figure 5 (further details are presented in Table S1). For the individual Phe residues of KFFE, there is a significant preference for one of the states to occur, with 1+ and 2− having the highest frequencies of observation (Table 1). The preference is the same for KVVE, but for KFFE, the bias in this conformational equilibrium is more pronounced. This suggests that the interaction of the bulkier Phe side chain with the rest of the molecule leads to larger differences in energy between the two conformational states compared to Val. To address interactions between the residues, we determined from the STM images the frequencies (Table S1) for observing the

TABLE 1. Statistical Occurrence of High/Low Conformational States in Individual Phe or Val Peptide Residues As Obtained from Analysis of STM Images (See Figure 4b for Definition of the Conformations)

	KFFE	KVVE
single conformations	observed single conformation frequencies (%)	observed single conformation frequencies (%)
2−	84.6	60.8
2+	15.4	39.2
1−	27.5	48.0
1+	72.5	52.0

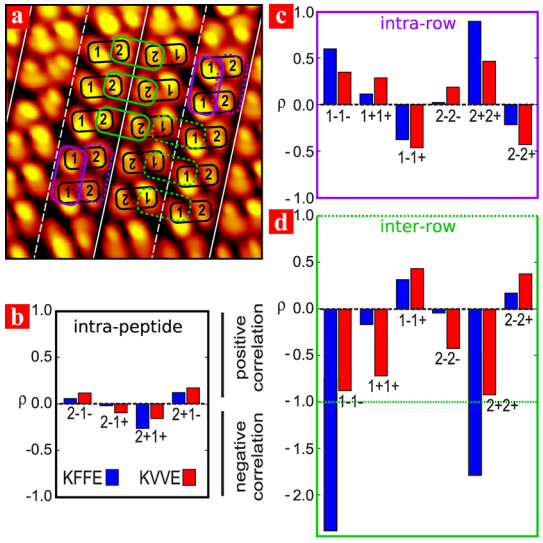

Figure 5. Correlations in the conformation assumed by Phe/Val residues in the KFFE/KVVE row structures. (a) STM image with overlaid contours to identify intramolecular (black), inter-row intermolecular (green), and intra-row intermolecular (purple) motifs analyzed for correlations. The single-residue conformations 1−, 1+, 2−, and 2+ are defined in Figure 4b. The correlation is defined as $\rho = \ln(f_{AB}/P_{AB})$, where f_{AB} is the observed frequency of two combined conformations (*e.g.*, AB = 2−1−) and P_{AB} is the uncorrelated probability for this event ($P_{AB} = f_A f_B$) calculated from the observed frequencies in Table 1 of conformations for the individual residues (see also Table S1). This measure is chosen since it provides symmetry between positively and negatively correlated situations. (b) Intramolecular correlations. (c) Intra-row correlations. (d) Inter-row correlations.

different possible combinations of conformations for neighboring residues, both intramolecularly and intermolecularly along and between the rows as defined in Figure 5a. These frequencies were compared to the uncorrelated probabilities for these events, calculated from the observed frequencies of conformations for the individual residues. Combinations with observed frequencies higher or lower than expected from the uncorrelated probabilities are referred to as positively and negatively correlated, respectively. From this detailed analysis (Figure 5), it is striking that the Phe and Val residues always show the same overall trend in the correlation. Importantly, this suggests that $\pi-\pi$ interactions do not dominate the ordering in these structures. Surprisingly, we observe that the intrapeptide correlations (Figure 5b) are weaker than the interpeptide correlations (Figure 5c,d). The conformations of the two Phe/Val residues within a peptide unit are thus not correlated, which could indicate that they point away from each other. Conversely, between the rows (Figure 5d), we observe that homo configurations are negatively correlated (*e.g.*, a 1− conformation avoids being combined with a neighboring 1−), suggesting a possible steric clash for certain homo configurations. These two findings are supported by the MDFF models in which Phe side chains of the same peptide have little interaction, whereas the side chain between different rows is in much closer contact. Along the rows (Figure 5c) all homo configurations show positive correlations. This suggests a mechanism for fibril growth along the fibril axis by which new monomers are added and matches the conformation of the preceding unit to form a favorable interaction in a cooperative manner. On the basis of these STM results for the dynamics and correlations of the Phe residues, we propose that a thermodynamic equilibrium is established for the conformations during the gradual cool down to form the ordered peptide islands, and that the positive/negative correlations for homo conformations along/between the rows balance out, preventing complete conversion into a homogeneous structure.

CONCLUSION

We have investigated the surface self-assembly of two fibril-forming tetrapeptides under UHV conditions. Obviously, many factors relevant to fibril formation under actual hydrous conditions are not included when working in a UHV environment, such as interaction with solvent molecules and ions, pH, and hydrophobic interactions. As demonstrated here, however, we find the UHV-STM experiments useful to obtain insights into interactions and assembly processes relevant for amyloid fibril formation at the single-molecule level with submolecular resolution and with the possibility to reduce temperature to freeze out thermal motion of residues. In the present case of the tetrapeptides KFFE and KVVE, we find highly ordered self-assembled structures on an inert Au(111) surface with distinct parallel/antiparallel arrangements. Analysis of the STM data using MDFF methods, as commonly used for NMR structure determination, provides a basis for determining the structures of the individual molecules and analyzing determinants for their assembly into ordered structures. The U- and S-shaped structures of KFFE and KVVE as well as their parallel/antiparallel arrangement resemble earlier proposed fibril structures.[36,37] Statistical analysis of the STM data reveals different combinations of conformations for the Phe/Val residues and their dynamical transitions. Interestingly, interpeptide correlations for the residue

conformations are stronger than intrapeptide correlations, and these do not appear to be dominated by $\pi-\pi$ interactions. These single-molecule, local-probe observations suggest a mechanism for fibril growth in which new monomers are added and match the conformation of the preceding unit to form a favorable interaction in a cooperative manner. In a broader perspective, the demonstration that tetrapeptides can be sublimated *in vacuo* onto surfaces provides a new perspective on the many different ways in which peptides can self-assemble and provide a wider range of possibilities for structural design of peptide self-organized nanostructures on surfaces.[39]

EXPERIMENTAL SECTION

Preparation of Peptides. The peptides were synthesized on a Liberty microwave-assisted peptide synthesizer (CEM Corporation) on a 0.25 mmol scale utilizing the Fmoc/*t*-Bu strategy and purified by means of RP-HPLC. See Supporting Information for further details.

STM Measurements. The experiments were performed in an ultrahigh vacuum chamber (base pressure in the low 10^{-10} mbar region) equipped with standard facilities for sample preparation as well as a variable-temperature Aarhus-STM. An atomically clean Au(111) single-crystal surface was prepared by repeated cycles of Ar+ sputtering at 1.5 keV for 20 min followed by sample annealing at 850 K for 10 min, resulting in a well-ordered $(22 \times \sqrt{3})$ herringbone reconstruction. The tetrapeptides were sublimated from glass crucibles resistively heated to a temperature of 426 K (KFFE) and 470 K (KVVE). Both molecular powders were thoroughly degassed prior to evaporation. After deposition of submonolayer quantities of tetrapeptides onto the Au(111) surface held at room temperature, the molecular adsorption structures were studied with STM in the temperature range of 125−180 K. The imaging was performed in constant current mode ($I_t \approx 0.4$ nA) at a bias voltage of $V_t \approx -1.25$ V with respect to the sample.

MDFF Calculations. Models of the row and antiparallel structure were calculated with the Xplor-NIH package[29] using standard procedures for restrained simulated annealing. Further details are provided in the main text and in the Supporting Information.

Conflict of Interest: The authors declare no competing financial interest.

Acknowledgment. We acknowledge financial support from the Marie-Curie EST MONET and ITN SMALL, The Danish Council for Independent Research Natural Sciences, The Villum Foundation, and the Danish National Research Foundation for support to the Sino-Danish Center for Molecular Nanostructures on Surfaces and Center for Insoluble Protein Structures (inSPIN). We acknowledge support from the Danish Center for Scientific Computing.

Supporting Information Available: Supporting methods section and supporting figures and tables. This material is available free of charge *via* the Internet at http://pubs.acs.org.

REFERENCES AND NOTES

1. Dobson, C. M. Protein Folding and Misfolding. *Nature* **2003**, *426*, 884–890.
2. Makin, O. S.; Atkins, E.; Sikorski, P.; Johansson, J.; Serpell, L. C. Molecular Basis for Amyloid Fibril Formation and Stability. *Proc. Natl. Acad. Sci. U.S.A.* **2005**, *102*, 315–320.
3. Sachse, C.; Fandrich, M.; Grigorieff, N. Paired β-Sheet Structure of an Aβ(1−40) Amyloid Fibril Revealed by Electron Microscopy. *Proc. Natl. Acad. Sci. U.S.A.* **2008**, *105*, 7462–7466.
4. Zhang, R.; Hu, X. Y.; Khant, H.; Ludtke, S. J.; Chiu, W.; Schmid, M. F.; Frieden, C.; Lee, J. M. Interprotofilament Interactions between Alzheimer's Aβ_{1-42} Peptides in Amyloid Fibrils Revealed by CryoEM. *Proc. Natl. Acad. Sci. U.S.A.* **2009**, *106*, 4653–4658.
5. Jaroniec, C. P.; MacPhee, C. E.; Bajaj, V. S.; McMahon, M. T.; Dobson, C. M.; Griffin, R. G. High-Resolution Molecular Structure of a Peptide in an Amyloid Fibril Determined by Magic Angle Spinning NMR Spectroscopy. *Proc. Natl. Acad. Sci. U.S.A.* **2004**, *101*, 711–716.
6. Petkova, A. T.; Leapman, R. D.; Guo, Z. H.; Yau, W. M.; Mattson, M. P.; Tycko, R. Self-Propagating, Molecular-Level Polymorphism in Alzheimer's β-Amyloid Fibrils. *Science* **2005**, *307*, 262–265.
7. Nielsen, J. T.; Bjerring, M.; Jeppesen, M. D.; Pedersen, R. O.; Pedersen, J. M.; Hein, K. L.; Vosegaard, T.; Skrydstrup, T.; Otzen, D. E.; Nielsen, N. C. Unique Identification of Supramolecular Structures in Amyloid Fibrils by Solid-State NMR Spectroscopy. *Angew. Chem., Int. Ed.* **2009**, *48*, 2118–2121.
8. Wasmer, C.; Lange, A.; Van Melckebeke, H.; Siemer, A. B.; Riek, R.; Meier, B. H. Amyloid Fibrils of the HET-s(218−289) Prion Form a β Solenoid with a Triangular Hydrophobic Core. *Science* **2008**, *319*, 1523–1526.
9. Adamcik, J.; Jung, J.-M.; Flakowski, J.; De Los Rios, P.; Dietler, G.; Mezzenga, R. Understanding Amyloid Aggregation by Statistical Analysis of Atomic Force Microscopy Images. *Nat. Nanotechnol.* **2010**, *5*, 423–428.
10. Bleiholder, C.; Dupuis, N. F.; Wyttenbach, T.; Bowers, M. T. Ion Mobility−Mass Spectrometry Reveals a Conformational Conversion from Random Assembly to β-Sheet in Amyloid Fibril Formation. *Nat. Chem.* **2011**, *3*, 172–177.
11. Ma, X. J.; Liu, L.; Mao, X. B.; Niu, L.; Deng, K.; Wu, W. H.; Li, Y. M.; Yang, Y. L.; Wang, C. Amyloid β (1−42) Folding Multiplicity and Single-Molecule Binding Behavior Studied with STM. *J. Mol. Biol.* **2009**, *388*, 894–901.
12. Mao, X. B.; Ma, X. J.; Liu, L.; Niu, L.; Yang, Y. L.; Wang, C. Structural Characteristics of the β-Sheet-like Human and Rat Islet Amyloid Polypeptides as Determined by Scanning Tunneling Microscopy. *J. Struct. Biol.* **2009**, *167*, 209–215.
13. Mao, X. B.; Wang, Y. B.; Liu, L.; Niu, L.; Yang, Y. L.; Wang, C. Molecular-Level Evidence of the Surface-Induced Transformation of Peptide Structures Revealed by Scanning Tunneling Microscopy. *Langmuir* **2009**, *25*, 8849–8853.
14. Lepère, M.; Chevallard, C.; Brezesinski, G.; Goldmann, M.; Guenoun, P. Crystalline Amyloid Structures at Interfaces. *Angew. Chem., Int. Ed.* **2009**, *48*, 5005–5009.
15. Whitehouse, C.; Fang, J. Y.; Aggeli, A.; Bell, M.; Brydson, R.; Fishwick, C. W. G.; Henderson, J. R.; Knobler, C. M.; Owens, R. W.; Thomson, N. H.; *et al.* Adsorption and Self-Assembly of Peptides on Mica Substrates. *Angew. Chem., Int. Ed.* **2005**, *44*, 1965–1968.
16. Liu, L.; Busuttil, K.; Zhang, S.; Yang, Y.; Wang, C.; Besenbacher, F.; Dong, M. The Role of Self-Assembling Polypeptides in Building Nanomaterials. *Phys. Chem. Chem. Phys.* **2011**, *13*, 17435–17444.
17. Mao, X.-B.; Wang, C.-X.; Wu, X.-K.; Ma, X.-J.; Liu, L.; Zhang, L.; Niu, L.; Guo, Y.-Y.; Li, D.-H.; Yang, Y.-L.; *et al.* Beta Structure Motifs of Islet Amyloid Polypeptides Identified through Surface-Mediated Assemblies. *Proc. Natl. Acad. Sci. U.S.A.* **2011**, DOI: 10.1073/pnas.1102971108.
18. Ghiringhelli, L. M.; Hess, B.; van der Vegt, N. F. A.; Delle Site, L. Competing Adsorption between Hydrated Peptides and Water onto Metal Surfaces: From Electronic to Conformational Properties. *J. Am. Chem. Soc.* **2008**, *130*, 13460–13464.
19. Marti, E. M.; Quash, A.; Methivier, C.; Dubot, P.; Pradier, C. M. Interaction of S-Histidine, an Amino Acid, with Copper and Gold Surfaces, a Comparison Based on RAIRS Analyses. *Colloids Surf., A* **2004**, *249*, 85–89.

20. Schiffrin, A.; Riemann, A.; Auwärter, W.; Pennec, Y.; Weber-Bargioni, A.; Cvetko, D.; Cossaro, A.; Alberto, M.; Barth, J. V. Zwitterionic Self-Assembly of L-Methionine Nanogratings on the Ag(111) Surface. *Proc. Natl. Acad. Sci. U.S.A.* **2007**, *104*, 5279–5284.
21. Kühnle, A.; Linderoth, T. R.; Hammer, B.; Besenbacher, F. Chiral Recognition in Dimerization of Adsorbed Cysteine Observed by Scanning Tunnelling Microscopy. *Nature* **2002**, *415*, 891–893.
22. Chen, Q.; Richardson, N. V. Enantiomeric Interactions between Nucleic Acid Bases and Amino Acids on Solid Surfaces. *Nat. Mater.* **2003**, *2*, 324–328.
23. Stensgaard, I. Adsorption of Di-L-Alanine on Cu(110) Investigated with Scanning Tunneling Microscopy. *Surf. Sci.* **2003**, *545*, L747–L752.
24. Lingenfelder, M.; Tomba, G.; Costantini, G.; Ciacchi, L. C.; De Vita, A.; Kern, K. Tracking the Chiral Recognition of Adsorbed Dipeptides at the Single-Molecule Level. *Angew. Chem., Int. Ed.* **2007**, *46*, 4492–4495.
25. Tomba, G.; Lingenfelder, M.; Costantini, G.; Kern, K.; Klappenberger, F.; Barth, J. V.; Ciacchi, L. C.; De Vita, A. Structure and Energetics of Diphenylalanine Self-Assembling on Cu(110). *J. Phys. Chem. A* **2007**, *111*, 12740–12748.
26. Wang, Y.; Lingenfelder, M.; Classen, T.; Costantini, G.; Kern, K. Ordering of Dipeptide Chains on Cu Surfaces through 2D Cocrystallization. *J. Am. Chem. Soc.* **2007**, *129*, 15742–15743.
27. Tjernberg, L.; Hosia, W.; Bark, N.; Thyberg, J.; Johansson, J. Charge Attraction and β Propensity Are Necessary for Amyloid Fibril Formation from Tetrapeptides. *J. Biol. Chem.* **2002**, *277*, 43243–43246.
28. Wolf, M. G.; Jongejan, J. A.; Laman, J. D.; de Leeuw, S. W. Quantitative Prediction of Amyloid Fibril Growth of Short Peptides from Simulations: Calculating Association Constants To Dissect Side Chain Importance. *J. Am. Chem. Soc.* **2008**, *130*, 15772–15773.
29. Schwieters, C. D.; Kuszewski, J. J.; Tjandra, N.; Clore, G. M. The Xplor-NIH NMR Molecular Structure Determination Package. *J. Magn. Reson.* **2003**, *160*, 65–73.
30. Wüthrich, K. Protein-Structure Determination in Solution by NMR-Spectroscopy. *J. Biol. Chem.* **1990**, *265*, 22059–22062.
31. Kirkpatrick, S.; Gelatt, C. D.; Vecchi, M. P. Optimization by Simulated Annealing. *Science* **1983**, *220*, 671–680.
32. Metropolis, N.; Rosenbluth, A. W.; Rosenbluth, M. N.; Teller, A. H.; Teller, E. Equation of State Calculations by Fast Computing Machines. *J. Chem. Phys.* **1953**, *21*, 1087–1092.
33. Bellesia, G.; Shea, J.-E. What Determines the Structure and Stability of KFFE Monomers, Dimers, and Protofibrils? *Biophys. J.* **2009**, *96*, 875–886.
34. Strodel, B.; Wales, D. J. Implicit Solvent Models and the Energy Landscape for Aggregation of the Amyloidogenic KFFE Peptide. *J. Chem. Theory Comput.* **2008**, *4*, 657–672.
35. Baumketner, A.; Shea, J.-E. Free Energy Landscapes for Amyloidogenic Tetrapeptides Dimerization. *Biophys. J.* **2005**, *89*, 1493–1503.
36. Geddes, A. J.; Parker, K. D.; Atkins, E. D.; Beighton, E. "Cross-β" Conformation in Proteins. *J. Mol. Biol.* **1968**, *32*, 343–358.
37. Sawaya, M. R.; Sambashivan, S.; Nelson, R.; Ivanova, M. I.; Sievers, S. A.; Apostol, M. I.; Thompson, M. J.; Balbirnie, M.; Wiltzius, J. J. W.; McFarlane, H. T.; *et al.* Atomic Structures of Amyloid Cross-β Spines Reveal Varied Steric Zippers. *Nature* **2007**, *447*, 453–457.
38. IUPAC-IUB Commission on Biochemical Nomenclature. Abbreviations and Symbols for the Description of the Conformation of Polypeptide Chains. Tentative Rules (1969). *Biochemistry* **1970**, *9*, 3471−3479.
39. Zhao, X.; Pan, F.; Xu, H.; Yaseen, M.; Shan, H.; Hauser, C. A. E.; Zhang, S.; Lu, J. R. Molecular Self-Assembly and Applications of Designer Peptide Amphiphiles. *Chem. Soc. Rev.* **2010**, *39*, 3480–3498.